Su L, Blamire AM, Watson R, He JB, Aribisala B, O'Brien JT.

Cortical and Subcortical Changes in Alzheimer's Disease: A Longitudinal and Quantitative MRI Study.

***Current Alzheimer Research* 2016, 13(5), 534-544.**

Cortical and subcortical changes in Alzheimer's disease: a longitudinal and quantitative MRI study

Li Su[1], Andrew M. Blamire[2], Rosie Watson[3], Jiabao He[4], Benjamin Aribisala[5], and John T. O'Brien[1]

1. Department of Psychiatry, University of Cambridge, Cambridge Biomedical Campus, Cambridge, UK;
2. Institute of Cellular Medicine & Newcastle Magnetic Resonance Centre, Newcastle University, Newcastle upon Tyne, UK;
3. Aged Care Department, Royal Melbourne Hospital, Parkville, Australia;
4. The Institute of Medical Sciences, University of Aberdeen, Aberdeen, UK;
5. Division of Clinical Neurosciences, Western General Hospital, University of Edinburgh, Edinburgh, UK

Correspondence to

Dr. Li Su

Department of Psychiatry,

School of Clinical Medicine, University of Cambridge

Box 189, Level E4, Cambridge Biomedical Campus

Cambridge, UK, CB2 0SP

Email: ls514@cam.ac.uk

Tel: +44(0)1223331134

Short title: Longitudinal and quantitative MRI in AD

Abstract

Quantitative MRI provides important information about tissue properties in brain both in normal ageing and in degenerative disorders. Although it is well known that those with Alzheimer's disease (AD) show a specific pattern and faster rate of atrophy than controls, the precise spatial and temporal patterns of quantitative MRI in AD are unknown. We aimed to investigate neuroimaging correlates of AD using serial quantitative MRI. In our study, twenty-one subjects with AD and thirty-two similar-aged healthy controls underwent two serial MRI scans at baseline and 12 months. Tissue characteristics were captured using two quantitative MRI parameters: longitudinal relaxation time (qT1) and transverse relaxation time (qT2). The two groups (AD and controls) were statistically compared using a voxel based quantification (VBQ) method based on Matlab and SPM8. At baseline, subjects with AD showed a significant reduction of qT1 and qT2 compared to controls in bilateral temporal and parietal lobes, hippocampus, and basal ganglia. This pattern was also observed at follow-up. Longitudinally, in AD we found a significant increase rather than further reduction of qT1 and qT2 from the baseline in bilateral hippocampus, thalamus and right caudate nucleus. In addition, the longitudinal change of qT1 in left hippocampus was negatively correlated with cognitive decline in AD over the 1-year period, and the general disease severity significantly predicted the amount of increase of qT1 in bilateral hippocampus over 12 months. The longitudinal change of qT2 in left parahippocampus correlated with change in neuropsychiatric features over time. In summary, quantitative MRI parameters were reduced in AD cross-sectionally, but increased over time, showing distinct spatiotemporal patterns

from the atrophy in AD. We also showed the clinical relevance of quantitative MRI parameters, indicating their potential promise as new imaging markers in AD.

(286 words)

Keywords quantitative MRI, VBQ, Alzheimer's disease, amyloid, relaxometry, early diagnostics

Introduction

One of the main current research focuses on Alzheimer's disease (AD) is early intervention, thus, there is a pressing need for reliable biomarkers for early AD detection. Existing biomarkers include cerebrospinal fluid (CSF), PET/SPECT imaging of neural metabolism and β-amyloid binding, as well as structural and functional MRI [1]. Among these techniques, MRI is noninvasive, so provides a powerful and safe tool for research and clinical diagnosis / screening, both of which are important for investigating the underlying neuropathology and early detection [2].

It has been shown that MRI not only reveals changes in brain volume and macrostructure, but also microstructural alterations in brain tissue integrity and its biochemical environment [3]. An emerging neuroimaging technique is quantitative MRI (qMRI) based on the physical measurement of longitudinal (qT1) and transverse (qT2) relaxation times. (Here we shall refer to these quantitative measurements as qT1 and qT2 to distinguish them from the more common qualitative radiological T1 or T2 weighted scans). In general, qT1 is correlated with water content and the level of myelination, and qT2 is related to chemically determined brain iron concentration [3].

Quantitative MRI provides important information about tissue properties in brain both in normal ageing [4,5], degenerative disorders such as Parkinson's disease [6], AD and dementia with Lewy bodies (DLB) [7], and neuronal loss due to brain and spinal cord injury [8]. In our previous study of DLB using qMRI, we demonstrated that the spatial pattern in the changes of qT1 and

qT2 was different from the pattern of atrophy, thus quantitative MRI may provide incremental benefit over and above that of structural MRI [7]. We also argue that quantitative MRI may indirectly detect neuronal and molecular changes in AD that precede the structural brain damage and clinical impairments decades in time [2]. Although it is well known that those with AD show a specific pattern and faster rate of atrophy than controls, the precise spatial and temporal patterns of quantitative MRI alteration in AD are unknown.

In this study, we aimed to investigate neuroimaging correlates of AD using serial quantitative MRI. In particular, we evaluated maps of qT1 and qT2 in grey matter comparing these parameters between the AD and the similarly aged control groups using the voxel-based quantification (VBQ) approach [4] both cross-sectionally and longitudinally. In addition, we explored the clinical relevance of quantitative MRI changes over a 12-month period.

Materials and Methods

Subjects, assessment and diagnosis

Thirty-six subjects with probable AD [9] over the age of 60 were recruited from a community dwelling population of patients referred to local Old Age Psychiatry, Geriatric Medicine or Neurology Services. Thirty-five similarly aged control subjects were recruited from relatives and friends of subjects with dementia or volunteered via advertisements in local community newsletters. Twenty-one AD subjects and 32 controls underwent MR imaging

at both baseline and follow-up and are included in the analyses reported here. These subjects underwent clinical and neuropsychological evaluations at baseline and follow-up at 1 year. (The rest of subjects were not scanned at follow-up, thus excluded from the analysis.)

The research was approved by Newcastle & North Tyneside 1 Research Ethics Committee (No. 05/Q0905/217). All subjects or, where appropriate, their nearest relative, provided written informed consent. Assessment of global cognitive measures at both baseline and follow-up assessments included the Cambridge Cognitive Examination (CAMCOG) [10], which incorporates the Mini-Mental State Examination (MMSE) [11]. Motor parkinsonism was evaluated with the Unified Parkinson's Disease Rating Scale Part III (UPDRS-III) [12]. For subjects with dementia, neuropsychiatric features were evaluated with the Neuropsychiatric Inventory (NPI) [13].

MRI data acquisition

Participants underwent MRI scanning on a 3T Philips Achieva MRI system with an 8-channel receiver head coil at both baseline and 12-month follow-up. Structural images were acquired using a T1 weighted volumetric sequence (3D MPRAGE, sagittal acquisition aligned with the AC-PC line, 1mm isotropic resolution, matrix 240×240×180, TR=9.6ms, TE=4.6ms, flip angle=8^{o}, SENSE factor 2). In addition, a B0 field-map using a dual echo 3D GRE (2mm isotropic resolution, matrix 128×128×72, TR=27ms, TE=2.6/6.1ms) was acquired.

Quantitative mapping of tissue qT1 and qT2 relaxation times was performed using custom designed MRI sequences developed in-house under a research agreement with Philips Medical Systems.

Fast qT1 mapping was based on the inversion recovery (IR) methods originally published by Ordidge et al [14] and expanded by Clare and Jezzard [15]. The sequence imaged 72 axial slices spanning the brain, which were grouped into 5 consecutive slabs each of thickness 24mm. For each slab a slice selective adiabatic (sech) inversion pulse was applied to invert the magnetisation ensuring that the region of full inversion encompassed the 24 mm thick section of interest. This inversion was followed by slice selective single shot EPI readout of 12 contiguous slices of 2 mm thickness equally spaced across the slab. The first slice was imaged 250ms post inversion and subsequent slices every 205 ms thereafter. During the repetition time (TR) of 15000ms each slab was inverted and imaged with a slab order of 1,3,5,2,4 to minimise interaction between slices. In this way the time between inverting adjacent slabs was 6000ms, sufficient to allow full relaxation of brain tissue. The sequence was repeated 12 times and on each repetition the order of acquired slices within each slab was permuted by one position, for example

1,2,3,4,5,6,7,8,9,10,11,12

2,3,4,5,6,7,8,9,10,11,12,1

3,4,5,6,7,8,9,10,11,12,1,2

etc

such that the at the end of acquisitions every slice had been imaged at each

of the 12 inversion times. Total scan time was therefore 180s for the complete IR series in 72 slices with isotropic 2mm resolution. This sequence is shown schematically in Figure 1.

Insert Figure 1 here

Calculation of qT1 maps used a purpose written algorithm in Matlab, which reordered the data into incremental inversion order for each slice and then performed voxel-wise non-linear least squares fitting to the standard 3 parameter model for the inversion recovery experiment:

$$S(T_{IR}) = S_o(1 - \alpha e^{\frac{-T_{IR}}{qT1}})$$

where T_{IR} is the inversion time, $S(T_{IR})$ is the signal value or the data obtained from the inversion recovery experiment, qT1 is the longitudinal relaxation time, S_o is the proton density and α is the effective inversion efficiency . qT1, S_o and α were computed pixel-wise from the fitting process. Ideally α is expected to be 2 but it was allowed to be a free variable in the fitting in order to increase the accuracy of the computed qT1. The 3D images of proton density S_0, qT1, and the goodness of fit were saved for evaluation.

Fast qT2 mapping used a multi-spin echo sequence with segmented EPI readout based around a Gradient and Spin Echo Imaging sequence. The sequence collected 8 spin echoes with equal spacing of 20ms and 5 gradient recalled echoes per spin echo (EPI factor 5) to accelerate image collection.

Repetition time was set to 4700ms and 72 slices were collected in standard interleaved acquisition (2mm isotropic resolution, matrix 128×128). Total scan time was 120s.

Calculation of qT2 maps again used a purpose written algorithm in Matlab, which performed voxel-wise non-linear least squares fitting to the standard 2 parameter model for transverse relaxation.

$$S(TE) = S_o e^{\frac{-TE}{qT2}}$$

where *TE* is the echo time, qT2 is the transverse relaxation time and S_o is the proton density. qT2, and S_o were computed pixel-wise from the fitting process. The 3D images of proton density S_o, qT2, and the goodness of fit were saved for evaluation.

Scans were collected using both sequences in aqueous and gel based test objects of known qT1 and qT2 and compared to data collection using a single slice inversion recovery sequence for qT1 and a single slice Carr-Purcell Meiboom-Gill (CPMG) sequence for qT2 to validate the method.

Statistical Tests of Demographic, clinical, and cognitive measures.

Group characteristics were evaluated with Statistical Toolbox of Matlab (www.mathworks.co.uk/products/statistics). Differences in demographic and clinical data were assessed with use of either t-tests for continuous variables

or χ^2 tests for categorical measures. For each test statistic, a probability value of $p<0.05$ was regarded as significant.

Voxel-based quantification

MRI data processing was performed in a combined FSL (fsl.fmrib.ox.ac.uk/fsl/fslwiki) and SPM (www.fil.ion.ucl.ac.uk/spm) based on the previously validated voxel-based quantification (VBQ) procedure [4]. At both baseline and follow-up, raw qT1 and qT2 imaging datasets were corrected for field inhomogeneities using B0 maps and the PRELUDE/FUGUE algorithm in FSL [16]. Then, the bias corrected qT1 and qT2 maps were used for subsequent analysis.

Volumetric structural T1 weighted images were firstly segmented using Gaussian mixture model implemented in the VBM toolbox [17], and brain tissues were classified into grey matter (GM), white matter (WM) and Cerebrospinal fluid (CSF) for both baseline and follow-up. A conjunction GM brain mask was generated for each individual subject (in both AD and control groups) by computing the intersection between the GM probability maps at the baseline and that at the follow-up of the same subject, and then thresholded at $p>0.5$ in each participant's native space. This mask was used to select a common area of GM tissue at both baseline and follow-up in order to ensure there were equal number of voxels tested in both time points, thus avoiding potential bias in the statistical analysis.

As in standard longitudinal VBM procedure, only the baseline GM probability maps were non-linearly normalized to standard MNI space (www.mni.mcgill.ca) using the diffeomorphic registration algorithm (DARTEL) [17] in SPM, and the resulting parameters were used to normalize the qT1 and qT2 maps in both baseline and follow-up. The qT1 and qT2 maps at both time points were firstly co-registered with the GM probability maps derived from structural T1 images at baseline, then the thresholded conjunction GM brain masks were applied to qT1 and qT2 data at both time points. Finally, we transformed the GM maps of qT1 and qT2 MRI parameters into standard MNI space using the participant-specific diffeomorphic parameters estimated from the baseline scans based on the previous DARTEL procedure. However, we did not apply modulation to these quantitative MRI parameters in order to avoid confound of age and disease related GM volume changes. Finally, all normalized quantitative qT1 and qT2 maps were smoothed with an isotropic Gaussian kernel of 6 mm full width at half maximum.

For statistical analysis investigating disease induced regional microstructural alterations between the AD and control groups, and between the baseline and follow-up, we used the General Linear Model (GLM) with age and gender as covariates. Then, two-tailed t-tests were performed at each voxel to detect voxel-wise difference between the groups or time points. We also tested the group x time interaction using a mixed model ANOVA. The false positive rate was controlled using family-wise error (FWE) correction for multiple comparisons, and thresholded at $p<0.05$ at the cluster level.

Post-hoc region-of-interest analysis

To explore the clinical relevance of qT1 and qT2, in a post-hoc region-of-interest (ROI) analysis, we extracted the averaged quantitative MRI values from significant clusters found in the longitudinal comparison. Here, we used the unsmoothed maps in order to preserve the original values of the MR parameters. Then, we correlated cognitive and clinical measures with the averaged quantitative MRI values extracted from the significant clusters obtained from the previous group comparisons. These measurements included the CAMCOG, MMSE, UPDRS III and NPI total scores. Multiple comparisons were controlled using Bonferroni correction for the number of ROIs.

Results

Demographic clinical and cognitive measures

As shown in Table 1, there were no significant differences between AD and control groups for age, sex and educational level. However, as expected, the two groups significantly different at both baseline and follow-up for UPDRS III, NPI, MMSE and CAMCOG scores with subjects with AD scoring poorer in all measures compared to the controls.

Insert Table 1 here

Cross-sectional comparison of qT1: AD vs. controls

As shown in Figure 2A and Table 2A, at the baseline, we found a significant decrease in qT1 for the AD group compared to controls (p<0.0001, FWE) in bilateral temporal, parietal and occipital lobes, as well as several subcortical / striatal nuclei. Largest significant clusters were within bilateral hippocampus, parahippocampus, cuneus, precuneus, caudate and putamen. At the follow-up, we found a very similar pattern of qT1 changes comparing between AD and control groups. See Figure 2B and Table 2B. No significant increase in qT1 was found for the AD group compared to controls at either baseline or follow-up.

Insert Table 2 here

Insert Figure 2 here

Cross-sectional comparison of qT2: AD vs. controls

For qT2 at the baseline, we also found a significant decrease for the AD group compared to controls (p<0.0001, FWE) in left superior and right middle temporal lobes, bilateral hippocampus and left parahippocampus as shown in Figure 3A and Table 3A. At the follow-up, we found a very similar pattern of qT2 changes comparing between AD and control groups except for a cluster covering left caudate, putamen and pallidum, and a right cuneus cluster, which were not seen at the baseline. See Figure 3B and Table 3B. No significant increase in qT2 was found for the AD group compared to controls at either baseline or follow-up.

Insert Table 3 here

Insert Figure 3 here

Longitudinal comparison of qT1: baseline vs. follow-up

When comparing qT1 between baseline and follow-up in the AD group, we found a significant increase over 12 months in bilateral hippocampus and parahippocampus (p<0.0001, FWE), thalamus (p<0.0001 for left and p=0.002 for right, FWE) and right caudate (p<0.0001, FWE) as shown in Figure 2C and Table 4A. The significant hippocampus clusters in the longitudinal comparison are more medial to the clusters found in the cross-sectional comparisons; see Figure 2. We found no longitudinal change for qT1 in the control group and no group (AD and controls) x time (baseline and follow-up) interaction.

Insert Table 4 here

Longitudinal comparison of qT2: baseline vs. follow-up

For qT2, we found a significant increase between the baseline and the follow-up in the AD group as shown in Figure 3C and Table 4B. Significant clusters are located in left parahippocampus (p<0.0001, FWE), right caudate, putamen and insula (p<0.0001, FWE), as well as right middle frontal lobe (p=0.002, FWE). We found a significant group x time interaction in right insula

(p<0.0001, FWE, Table 4C) bordering with right putamen and extending to right caudate at lower threshold (p<0.001, uncorrected). We argue that atrophy is unlike the explanation of this effect because if atrophy were a driver of an increase in qT2 over time, we would expect AD subjects at baseline to have a greater qT2 than controls because of their greater atrophy, a result opposite to what we found here.

For the control group, we found a significant longitudinal increase in qT2 (p<0.0001, FWE) in left superior parietal lobe, caudate head, and supplementary motor area extending to superior medial prefrontal cortex. (See Figure 3D.)

Correlation between cognitive / clinical measures and quantitative MRI

Here, the main focus is on the relationship between longitudinal changes in quantitative MRI parameters and cognitive / clinical measures in the AD group at baseline, follow-up and change over the 1-year period. Thus for qT1, we have defined three region-of-interest (ROIs) based on the results of the longitudinal comparison of qT1, i.e. left / right hippocampus and right caudate. We found a significant negative correlation between the longitudinal changes in qT1 in left hippocampus and the cognitive decline (i.e. change in total MMSE score over the 1-year period) in AD (r=-0.58, p=0.006). We found a significant correlation between baseline CAMCOG score and the changes of qT1 in bilateral hippocampus over the 1-year period. In addition, a significant correlation was found between baseline UPDRS III score and the longitudinal

changes of qT1 in bilateral hippocampus. Both effects were stronger in the right hemisphere than in the left and only the right hippocampus survived the correction for multiple comparisons. (See Table 5A.) Nonetheless, this suggests that baseline CAMCOG and UPDRS scores predict changes in qT1 in these regions, that is, the more severe the dementia in general, the more qT1 increases.

We also found a significant correlation between qT1 in right caudate and UPDRS score cross-sectionally at both baseline (r=0.60, *p*=0.004) and follow-up (r=0.51, *p*=0.018) in AD. Moreover, qT1 in right hippocampus was significantly correlated with the CAMCOG score only at the follow-up (r=-0.60, *p*=0.004) but not at the baseline. (See Table 5A.) No other correlation survived the correction for multiple comparisons.

Insert Table 5 here

For qT2, we have extracted qMRI values from four significant clusters found in the longitudinal comparison: right insula extending to putamen, left parahippocampus, right caudate and right superior medial frontal cortex (BA8). We found a significant correlation between the longitudinal changes of qT2 in left parahippocampus and the changes in NPI score over time (r=0.54, *p*=0.012) in AD. (See Table 5B.) No other correlation was found.

Individual analysis in longitudinal comparison

Figure 4 shows the individual variability in longitudinal changes in quantitative MRI within the AD group, and how it relates to disease severity. It can be seen in Figure 4A that subjects with AD showed a general increase in qT1 in right hippocampus, and the rate of increase seems to accelerate in moderate and severe cases of AD, i.e. baseline MMSE score lower than 20. The same pattern was observed in other clusters found in the longitudinal analysis. Figure 4B shows the individual changes in qT2 in left parahippocampus over time. We have found a very similar trend as in qT1 with subjects with AD generally showing an increase in qT2 over 12 months. We have also found similar pattern in other significant clusters derived in the longitudinal analysis in the AD group.

Insert Figure 4 here

Discussion

Using novel longitudinal and quantitative MRI method and voxel-based quantification, we showed that at the cross-sectional level, qT1 and qT2 in AD were significantly decreased in multiple cortical areas in bilateral temporal and parietal lobes with the largest changes in medial temporal structures comparing to similarly aged control subjects at baseline. This pattern is consistent with previous neuroimaging studies with AD showing significant volume reduction in these regions such as hippocampal, enthorinal and parahippocampal cortices [18].

At follow-up, we found a very similar pattern of quantitative MRI changes in both qT1 and qT2 comparing AD and control groups with the main affected brain areas in bilateral hippocampus and associated structures. This demonstrates the robustness of qMRI in reproducing a consistent pattern of quantitative MRI parameter changes at two different time points with 12 months gap.

It is worth noting that both qT1 and qT2 parameters consistently picked up substantial changes in subcortical regions, e.g. bilateral caudate, putamen and thalamus. However, comparing to neocortex, in particular the hippocampus, these basal nuclei and thalamus have received much less attention in previous research, and conventional volumetric MRI showed a mixed picture of atrophy in these subcortical areas. For example, atrophy of putamen was found in DLB but not in AD [19], whereas putamen and thalamic atrophy were both shown in AD in a different study [20] reflecting a relatively high level of noise in volumetric measures in these regions and large inter-study variability. In contrast, quantitative MRI may detect neuronal and macromolecular changes in tissue environment, which does not rely on atrophy shown in structural T1 weighted MRI. Based on this, we argue that qMRI provides incremental benefit over and above that of structural MRI. Quantitative MRI also offers a unique opportunity to detect early brain changes in AD before observable brain volume reduction can be reliably shown and cognitive / clinical impairments can be found [2].

Although we found that AD was characterized by a reduction in qMRI

parameters in cross-sectional comparison, in longitudinal comparison, we found that qT1 was increased rather than decreased in right caudate, bilateral hippocampus and parahippocampus, as well as in thalamus. We also found that qT2 was increased in right caudate, putamen and insula in addition to left parahippocampus in AD. Frontal changes in qT2 over time were also notable in AD. This spatial pattern is consistent with the development of atrophy in AD [21]. Increase in qT2 was found in healthy controls in left superior parietal lobe, left caudate head, and bilateral supplementary motor area extending to superior medial prefrontal cortex. However, none of these brain regions overlap with longitudinal qT1 / qT2 changes found in AD suggesting the increase of qT2 in AD and controls may reflect distinct underlying causes. The only significant group x time interaction was found in right insula extending to putamen and caudate nucleus.

To further understand the increase in qMRI over time in AD, we performed an individual analysis, which showed the changes of qT1 and qT2 over time in hippocampus, caudate and other clusters found in the longitudinal comparison. By sampling individual subjects that were at different stages of the disease indicated by their severity (i.e. baseline MMSE), we have pictured an overall trajectory of qT1 and qT2 in clinically diagnosed AD. It is notable that the rate of qMRI increase was slow at early stages of AD but accelerated at severe stage of AD. Thus, although qT1 and qT2 decreased in AD comparing with controls at the cross-section level, it is possible that qT1 and qT2 may increase over time in AD because plaque burden may stabilize or even fall in established stages of AD as the disease progresses. In addition,

we found that general disease severity (measured by different but related scales, i.e. CAMCOG and UPDRS) predicts the rate of change in qT1 in hippocampus showing a faster rate of increase at the severe stage of AD.

These changes in qMRI followed a trend that mirrors the inverted ‘U’ shape trajectory of brain β-amyloid over time [22] suggesting that at the severe stage of AD the brain β-amyloid (and/or other factors) may undergo a decrease. A more quantitative treatment of the parallels between the current results and the findings by Jack et al will require a deeper analysis of how the very different properties of the two might reflect how brain β-amyloid burden is captured by each imaging method, and the consequences of this for temporal trajectory of these variations. This analysis is outside the scope of the current paper, and the comparisons we provide here should be regarded as preliminary and illustrative. However, it is clear that such a ‘U’ shaped temporal pattern has not been found in atrophy in AD.

In addition, we showed the clinical relevance of quantitative MRI parameters in AD, i.e. the change of qT1 at left hippocampus was correlated with cognitive decline (annual changes in MMSE score) in AD. For qT2, the longitudinal change in right parahippocampus was significantly correlated with the annual changes in neuropsychiatry condition (NPI) in AD over time. In addition, we found a significant correlation between qT2 in right caudate nucleus and parkinsonism (UPDRS score) at the cross-sectional level (at both baseline and follow-up), suggesting the AD pathology may be present in basal ganglia structures, therefore causing motor parkinsonism in AD. Here, it is

interesting to see that qT2 in caudate was sensitive to the changes in UPDRS scores. This finding is also consistent with Wilson et al. [23], which showed that parkinsonian signs are strong predictors for the progression of AD.

In our previous cross-sectional study on dementia with Lewy bodies (DLB), we also found a significant reduction of qMRI parameters in DLB compared to controls [7]. In addition, we showed that the spatial pattern of qMRI alteration only partly overlapped with that of atrophy, making the latter an unlikely explanation for the qMRI decreases. In the current study, we have followed the similar analysis procedure in order to avoid partial volume effect due to atrophy. In seeking the possible underlying biochemical interpretation of these quantitative MRI parameters and their evolution over time, qT1 is predominantly influenced by water content but also relates to the degree of myelination [24,25,26]. Both qT1 and qT2 are also sensitive to the level of iron, which is present in amyloid plaques [27] and in microbleeds.

Although it is not possible to precisely determine the pathological changes associated with alterations in qT1 or qT2 in AD, it has been suggested that decreases in qT1 and qT2 might be associated with increases in amyloid burden and iron load in the brain based on histologically confirmed animal model of AD [28,29]. Consistent with our finding, decreased qT1 was found to be associated with an increase in β-amyloid deposition in 5xFAD transgenic mouse model of Alzheimer's disease compared with wild type mice [30]. In addition, decreased qT2 was found in APP/PS1 transgenic mouse model of

AD [31,32] probably reflecting a complex interaction between β-amyloid and iron concentration as well as other factors.

In a longitudinal study of β-amyloid plaque development in Tg2576 transgenic mice using qT2 relaxation time [33], it has been found that qT2 decreases with age (12 - 18 months) following an increase in plaque area, number and size in the brain. Although it is difficult to match the disease stage of the mouse model to humans with AD and it is not common to find atrophy in the animal model of AD, this finding is nonetheless consistent with our results showing decreased qT2 in medial temporal lobes in AD. It has also been shown in a study based on APP/PS1 transgenic mice model that qT2 is modulated by the level of amyloid in subiculum without histochemically detectable iron in the brain [34], providing promises in detecting the pathological process in AD at the earliest stages.

In addition to our previous findings on qMRI changes in DLB [7], as well as the established literature on animal qMRI correlates, the current data provided convergent evidence for the potential ability of quantitative MRI in detecting early changes of tissue property caused by neurodegenerative disease. Being able to apply this novel technique in human using relatively safe MRI method enables new means for early detection of AD and tracking its progression over time. This approach is also likely to close the gap between animal models of amyloidosis and studies on human AD in the context of drug discovery.

Conclusion

In summary, quantitative MRI parameters were reduced in AD cross-sectionally, but increased over time, showing distinct spatiotemporal patterns from the atrophy in AD. Our findings are consistent with animal model of AD showing quantitative MRI can provide information, which may reflect pathology such as amyloid burden and iron load. We also showed the clinical relevance of quantitative MRI, indicating their potential promise as new early imaging markers in AD. With reduced radiation, MRI is more suited for longitudinal studies than PET. Thus, longitudinal and quantitative MRI will be valuable in developing new treatments by tracking brain changes associated AD in vivo.

Acknowledgments

The study was funded by the Sir Jules Thorn Charitable Trust (grant ref: 05/JTA) and was supported by the National Institute for Health Research (NIHR) Newcastle Biomedical Research Centre and the Biomedical Research Unit in Lewy Body Dementia based at Newcastle upon Tyne Hospitals National Health Service (NHS) Foundation Trust and Newcastle University and the NIHR Biomedical Research Centre and Biomedical Research Unit in Dementia based at Cambridge University Hospitals NHS Foundation Trust and the University of Cambridge. The views expressed are those of the authors and not necessarily those of the NHS, the NIHR or the Department of Health. L. Su, A. Blamire, R. Watson, J. He and B. Aribisala report no disclosures. J. O'Brien has been a consultant for GE Healthcare, Servier, and Bayer Healthcare and has received honoraria for talks from Pfizer, GE Healthcare, Eisai, Shire, Lundbeck, Lilly, and Novartis.

550 **Reference**

551

[1] Craig-Schapiro R, Fagan AM, Holtzman DM. Biomarkers of Alzheimer's Disease. Neurobiology of Disease 35(2): 128-140 (2009).

[2] Frisoni GB, Fox NC, Jack, CR, Scheltens P, Thompson PM. The clinical use of structural MRI in Alzheimer disease. Nature Reviews Neurology 6: 67-77 (2010).

[3] Tofts P. Quantitative MRI of the brain: measuring changes caused by disease. John Wiley & Sons Ltd (2003).

[4] Draganski B, Ashburner J, Hutton C, Kherif F, Frackowiak RS, Helms G, *et al*. Regional specificity of MRI contrast parameter changes in normal ageing revealed by voxel-based quantification (VBQ). NeuroImage 55: 1423-34 (2011).

[5] Callaghan MF, Freund P, Draganski B, Anderson E, Cappelletti M, Chowdhury R, *et al*. Widespread age-related differences in the human brain microstructure revealed by quantitative magnetic resonance imaging. Neurobiology of Aging 35(8): 1862-72 (2014).

[6] Bunzeck N, Singh-Curry V, Eckart C, Weiskopf N, Perry RJ, Bain PG, *et al*. Motor phenotype and magnetic resonance measures of basal ganglia iron levels in Parkinson's disease. Parkinsonism and Related Disorders 19(12): 1136-42 (2013).

[7] Su L, Blamire AM, Watson R, He J, Aribisala B, O'Brien JT. Tissue microstructural changes in dementia with Lewy bodies revealed by quantitative MRI. Journal of Neurology 262(1): 165-72 (2014).

[8] Freund P, Weiskopf N, Ashburner J, Wolf K, Sutter R, Altmann DR, *et al*. MRI investigation of the sensorimotor cortex and the corticospinal tract after acute spinal cord injury: A prospective longitudinal study. Lancet Neurology 12(9): 873-81 (2013).

[9] McKhann G, Drachman D, Folstein M, Katzman R, Price D, Stadlan E. Clinical diagnosis of Alzheimer's disease: Report of the NINCDS-ADRDA Work Group* under the auspices of Department of Health and Human Services Task Force on Alzheimer's Disease. Neurology 34(7): 939-44 (1984).

[10] Huppert FA, Brayne C, Gill C, Paykel ES, Beardsall L. CAMCOG--a concise neuropsychological test to assist dementia diagnosis: socio-demographic determinants in an elderly population sample. Br J Clin Psychol 34(4): 529–41 (1995).

[11] Folstein MF, Folstein SE, McHugh PR. "Mini-mental state". A practical method for grading the cognitive state of patients for the clinician. J Psychiatr Res 12(3): 189–98 (1975).

[12] The Unified Parkinson's Disease Rating Scale (UPDRS): status and recommendations. Mov Disord 18(7): 738–50 (2003).

[13] Cummings JL, Mega M, Gray K, Rosenberg-Thompson S, Carusi DA, Gornbein J. The Neuropsychiatric Inventory: comprehensive assessment of psychopathology in dementia. Neurology 44(12): 2308-14 (1994).

[14] Ordidge RJ, Gibbs P, Chapman B, Stehling MK, Mansfield P. High-speed multislice T1 mapping using inversion-recovery echo-planar imaging. Magnetic Resonance in Medicine 16(2): 238-45 (1990).

[15] Clare S, Jezzard P. Rapid T-1 mapping using multislice echo planar imaging. Magnetic Resonance in Medicine 45: 630-34 (2001).

[16] Jenkinson M, Beckmann CF, Behrens TEJ, Woolrich MW, Smith SM. FSL. NeuroImage 62(2): 782-90 (2012).

[17] Ashburner J. A fast diffeomorphic image registration algorithm. NeuroImage 38: 95-113 (2007).

[18] Jack CR, Petersen RC, Xu YC, Waring SC, O'Brien PC, Tangalos EG, *et al*., Medial temporal atrophy on MRI in normal aging and very mild Alzheimer's disease. Neurology 49(3): 786-794 (1997).

[19] Cousins DA, Burton EJ, Burn D, Gholkar A, McKeith IG, O'Brien JT. Atrophy of the putamen in dementia with Lewy bodies but not Alzheimer's disease: an MRI study. Neurology 61(9): 1191-5 (2003).

[20] De Jong LW, van der Hiele K, Veer IM. Strongly reduced volumes of putamen and thalamus in Alzheimer's disease: an MRI study. Brian 131(12): 3277-3285 (2008).

[21] Matsuda H. Voxel-based Morphometry of Brain MRI in Normal Aging and Alzheimer's Disease. Aging Dis 4(1): 29–37 (2013).

[22] Jack CR, Wiste HJ, Lesnick TG, Weigand SD, Knopman DS, Vemuri P, *et al*., Brain β-amyloid load approaches a plateau. Neurology 80(10): 890-6 (2013).

[23] Wilson RS, Bennett DA, Gilley DW, Beckett LA, Schneider JA, Evans DA. Progression of parkinsonian signs in Alzheimer's disease. Neurology 54(6): 1284-9 (2000).

[24] Gelman N, Ewing JR, Gorell JM, Spickler EM, Solomon EG. Interregional variation of longitudinal relaxation rates in human brain at 3.0 T: relation to estimated iron and water contents. Magn Reson Med 45:71-79 (2001).

[25] MacKay A, Whittall K, Adler J, Li D, Paty D, Graeb D. In vivo visualization of myelin water in brain by magnetic resonance. Magn Reson Med 31: 673–7 (1994).

[26] Lutti A, Dick F, Sereno MI, Weiskopf N. Using high-resolution quantitative mapping of R1 as an index of cortical myelination. Neuroimage 93: 176-88 (2014).

[27] Fukunaga M, Li TQ, van Gelderen P, De Zwart JA, Shmueli K, Yao B, *et al*. Layer-specific variation of iron content in cerebral cortex as a source of MRI contrast. Proc Nat Acad Sci USA 107: 3834–9 (2010).

[28] Muskulus R Scheenstra AEH, Braakman N, Reiber JHC. Prospects for early detection of Alzheimer's disease from serial MRI images in transgenic mouse models. Current Alzheimer Research 6: 503-18 (2009).

[29] Adlard PA, Tran, BA, Finkelstein DI, Desmond PM., Johnston LA, Bush AI, *et al*. A review of β-amyloid neuroimaging in Alzheimer's disease. Frontiers in Neuroscience 8:327 (2014).

[30] Spencer NG, Bridgesb LR, Elderfield K, Amir K, Austen B, Howe FA. Quantitative evaluation of MRI and histological characteristics of the 5xFAD Alzheimer mouse brain. NeuroImage 76: 108-15 (2013).

[31] El Tannir El Tayara N, Delatour B, Le Cudennec C, Guegan M, Volk A, Dhenain M. Age-related evolution of amyloid burden, iron load, and MR relaxation times in a transgenic mouse model of Alzheimer's disease. Neurobiol Dis 22(1): 199-208 (2006).

[32] Chamberlain R, Reyes D, Curran GL, Marjanska M, Wengenack TM, Podusto JF, *et al*. Comparison of amyloid plaque contrast generated by T2-weighted, T2*-weighted, and susceptibility-weighted imaging methods in transgenic mouse models of Alzheimer's disease. Magn Reson Med 61(5): 1158-64 (2009).

[33] Braakman N, Matysik J, van Duinen SG, Verbeek F, Schliebs R, de Groot HJ, Alia A. Longitudinal assessment of Alzheimer's beta-amyloid plaque development in transgenic mice monitored by in vivo magnetic resonance microimaging. J Magn Reson Imaging 24(3): 530-6 (2006).

[34] El Tannir El Tayara N, Volk, A, Dhenain M, Delatour B. Transverse relaxation time reflects brain amyloidosis in young APP/PS1 transgenic mice. Magnetic Resonance in Medicine 58(1): 179-84 (2007).

Table 1. Demographics, clinical and neuropsychological measures.

Values expressed as Mean ± 1SD. Abbreviations: AD = Alzheimer's disease; HC = Healthy control; UPDRS III = Unified Parkinson's Disease Rating Scale, Part III; NPI Total = Neuropsychiatry Inventory; MMSE = Mini-Mental State examination; CAMCOG = Cambridge Cognitive Examination.

	HC (N=32)	AD (N=21)	p value
Gender (m:f)	19:13	12:9	X^2=0.03, p=0.87
Age (yrs)	76.6 ± 5.3	77.0 ± 5.4	t_{51}=-0.3, p=0.76
Education (yrs)	11.9 ± 2.7	11.5 ± 3.9	t_{51}=0.45, p=0.65
UPDRS III			
Baseline	1.8 ± 1.6	4.3 ± 3.5	t_{51}=-3.6, p<0.001
Follow-up	1.5 ± 1.7	5.1 ± 4.5	t_{51}=-4.1, p<0.001
NPI Total			
Baseline		19.7 ± 11.2	
Follow-up		15.5 ± 12.7	
MMSE			
Baseline	29.2 ± 0.9	20.6 ± 4.2	t_{51}=11.3, p<0.001
Follow-up	29.3 ± 0.9	19.2 ± 4.2	t_{51}=13.2, p<0.001
CAMCOG			
Baseline	97.9 ± 3.4	69.4 ± 12.1	t_{51}=12.7, p<0.001
Follow-up	98.5 ± 2.8	63.9 ± 15.0	t_{51}=12.8, p<0.001

Table 2 Significantly different clusters for qT1 at (A) baseline and (B) follow-up comparing the AD and control groups. FWE corrected, $p < 0.05$. (Only clusters with k > 300 are shown.)

Cluster level p FWE-Corr	Extent (k)	T	MNI coordinates (x,y,z)	Anatomical region
(A) baseline: Controls > AD				
< 0.0001	11950	10.06	30, -9, -18	Right hippocampus & parahippocampus
< 0.0001	12023	9.69	-34, -34, -9	Left hippocampus & parahippocampus
< 0.0001	1442	9.94	15, -69, 27	Right cuneus & precuneus
< 0.0001	759	6.52	21, 17, -5	Right caudate & putamen
< 0.0001	577	6.83	-12, -67, 21	Left cuneus & precuneus
< 0.0001	302	5.69	32, -76, 28	Right middle occipital lobe
(B) follow-up: Controls > AD				
< 0.0001	13161	9.69	30, -9, -18	Right hippocampus & parahippocampus
< 0.0001	9192	9.72	-34, -34, -9	Left hippocampus & parahippocampus
< 0.0001	997	7.53	-6, 8, -3	Left caudate & putamen
< 0.0001	620	6.64	21, 17, -5	Right caudate & putamen
< 0.0001	550	6.78	-14, -69, 19	Left cuneus & precuneus
< 0.0001	467	7.31	-26, -72, 36	Left superior occipital lobe
< 0.0001	393	7.24	-45, -58, 30	Left angular gyrus

Table 3 Significantly different clusters for qT2 at (A) baseline and (B) follow-up comparing the AD and control groups. FWE corrected, $p < 0.05$. (Only clusters with k > 50 are shown.)

Cluster level *p* FWE-Corr	Extent (k)	T	MNI coordinates (x,y,z)	Anatomical region
(A) baseline: Controls > AD				
< 0.0001	153	7.11	-34, -33, -9	Left hippocampus & parahippocampus
< 0.0001	103	7.09	30, -10, -17	Right hippocampus
< 0.0001	60	6.23	-51, -4, 1	Left superior temporal lobe
< 0.0001	59	6.48	-28, -10, -17	Left hippocampus
< 0.0001	55	6.71	60, -28, -2	Right middle temporal lobe
(B) followup: Controls > AD				
< 0.0001	229	7.12	-8, 9, -5	Left caudate, putamen & pallidum
< 0.0001	221	7.38	60, -28, -2	Right middle temporal lobe
< 0.0001	162	7.39	12, -70, 28	Right cuneus
< 0.0001	156	7.66	-33, -33, -8	Left hippocampus & parahippocampus
< 0.0001	65	6.19	62, -21, 13	Right middle temporal lobe
< 0.0001	62	5.84	24, 6, -24	Right hippocampus

Table 4 Significantly different clusters comparing the baseline and follow-up in the AD group for (A) qT1 and (B) qT2, as well as (C) significant time x group interaction for qT2. FWE corrected, $p < 0.05$. (Only clusters with k > 30 are shown when there is more than one cluster.)

Cluster level $p_{FWE\text{-}Corr}$	Extent (k)	T	MNI coordinates (x,y,z)	Anatomical region
(A) AD: follow-up > baseline for qT1				
< 0.0001	476	7.15	21, -6, 21	Right caudate
< 0.0001	327	6.73	28, -30, -8	Right hippocampus & parahippocampus
< 0.0001	114	6.97	-22, -37, -3	Left hippocampus & parahippocampus
< 0.0001	55	6.08	-6, -15, 10	Left thalamus
0.002	33	5.86	12, -19, 12	Right thalamus
(B) AD: follow-up > baseline for qT2				
< 0.0001	230	7.47	40, 3, -3	Right putamen & insula
< 0.0001	77	6.41	-24, -22, -24	Left parahippocampus
< 0.0001	64	5.91	18, -6, 21	Right caudate
0.002	30	5.86	30, 17, 49	Right middle frontal lobe (BA8)
(C) time x group interaction for qT2				
0.029	2	5.35	39, 3, -3	Right insula (extending to putamen and caudate at lower threshold of $p < 0.001$ uncorrected)

Table 5 Correlation between longitudinal changes in qT1 / qT2 and cognitive / clinical ratings in AD. Abbreviations: CAMCOG = Cambridge Cognitive Examination; MMSE = Mini-Mental State examination; UPDRS III = Unified Parkinson's Disease Rating Scale, Part III; NPI Total = Neuropsychiatry Inventory. ** significant correlation corrected for multiple comparisons, * significant correlation uncorrected.

(A) qT1

	Left hippocampus (follow-up - baseline)	Right hippocampus (follow-up - baseline)	Right caudate (follow-up - baseline)
CAMCOG (baseline)	r = -0.49, p = 0.026 *	r = -0.58, p = 0.006 **	r = -0.16, p = 0.492
CAMCOG (follow-up - baseline)	r = -0.37, p = 0.102	r = -0.27, p = 0.236	r = -0.30, p = 0.194
MMSE (baseline)	r = 0.006, p = 0.980	r = -0.29, p = 0.198	r = -0.09, p = 0.703
MMSE (follow-up - baseline)	r = -0.58, p = 0.006 **	r = -0.30, p = 0.183	r = -0.31, p = 0.167
UPDRS III (baseline)	r = 0.46, p = 0.035 *	r = 0.55, p = 0.009 **	r = 0.07, p = 0.764
UPDRS III (follow-up - baseline)	r = -0.05, p = 0.829	r = 0.08, p = 0.737	r = 0.13, p = 0.585
NPI (baseline)	r = 0.17, p = 0.469	r = 0.15, p = 0.521	r = 0.12, p = 0.595
NPI (follow-up – baseline)	r = -0.24, p = 0.290	r = -0.12, p = 0.593	r = 0.16, p = 0.492

(B) qT2

	Right putamen / insula (follow-up - baseline)	Left parahippocampus (follow-up - baseline)	Right caudate (follow-up - baseline)	Right BA8 (follow-up - baseline)
CAMCOG (baseline)	r = -0.30, p = 0.183	r = -0.19, p = 0.420	r = -0.24, p = 0.289	r = -0.27, p = 0.237
CAMCOG (follow-up - baseline)	r = -0.17, p = 0.459	r = 0.04, p = 0.879	r = 0.19, p = 0.414	r = -0.14, p = 0.548
MMSE (baseline)	r = -0.14, p = 0.537	r = -0.07, p = 0.748	r = -0.22, p = 0.339	r = -0.11, p = 0.640
MMSE (follow-up - baseline)	r = -0.21, p = 0.357	r = -0.09, p = 0.702	r = 0.15, p = 0.508	r = -0.07, p = 0.750

UPDRS III (baseline)	r = 0.007, p = 0.975	r = -0.15, p = 0.526	r = 0.16, p = 0.483	r = 0.13, p = 0.590
UPDRS III (follow-up - baseline)	r = -0.10, p = 0.681	r = 0.04, p = 0.871	r = -0.10, p = 0.656	r = -0.21, p = 0.353
NPI (baseline)	r = 0.13, p = 0.564	r = -0.12, p = 0.590	r = -0.22, p = 0.335	r = 0.30, p = 0.181
NPI (follow-up – baseline)	r = 0.16, p = 0.500	r = 0.54, p = 0.012 **	r = 0.10, p = 0.681	r = -0.02, p = 0.946

Figure 1 Schematic diagram of quantitative T1 mapping sequence

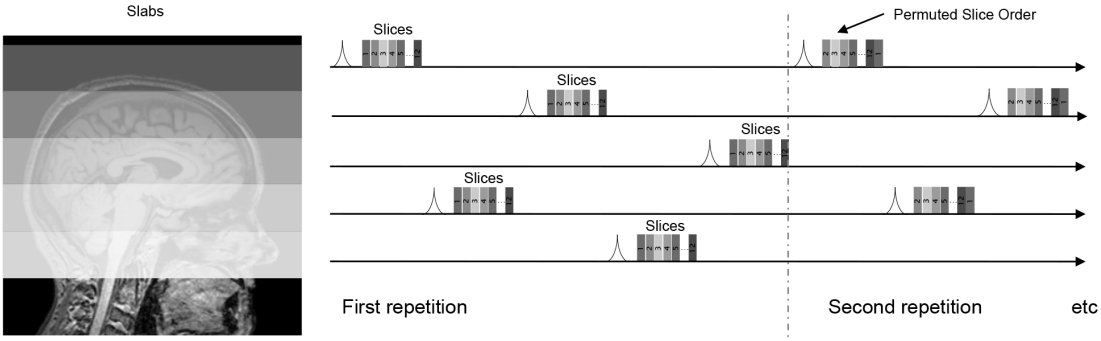

Figure 2 Significant clusters in the cross-sectional comparison showing the areas of qT1 decreases in AD compared to age matched controls at (A) baseline and (B) follow-up. (C) Significant clusters in the longitudinal comparison showing areas of qT1 increases in the AD group over time. FWE corrected, $p < 0.05$.

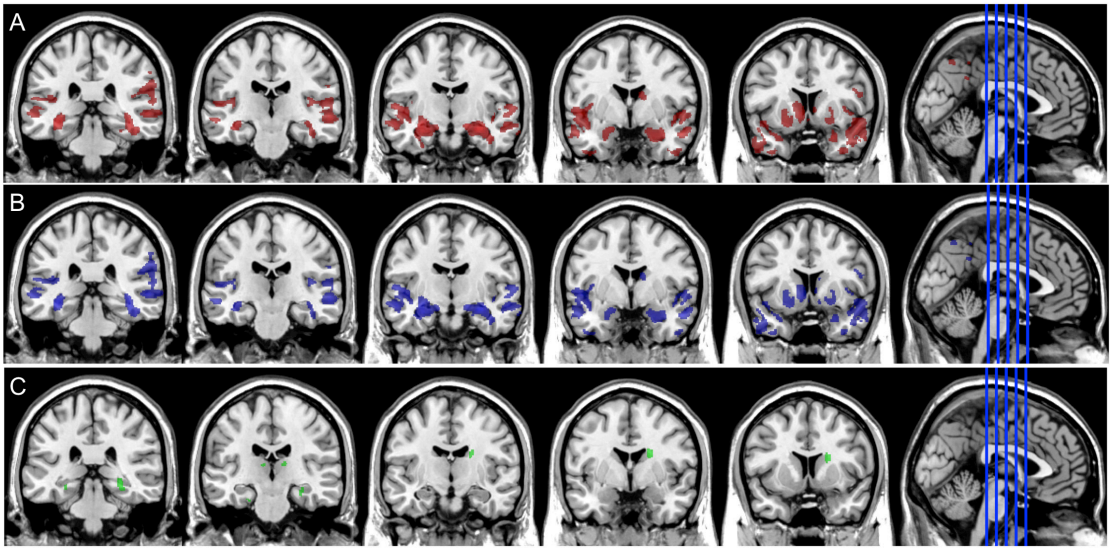

Figure 3 Significant clusters in the cross-sectional comparison showing the areas of qT2 decreases in AD compared to age matched controls at (A) baseline and (B) follow-up. Significant clusters in the longitudinal comparison showing areas of qT2 increases in (C) the AD and (D) the control groups over time. FWE corrected, $p < 0.05$.

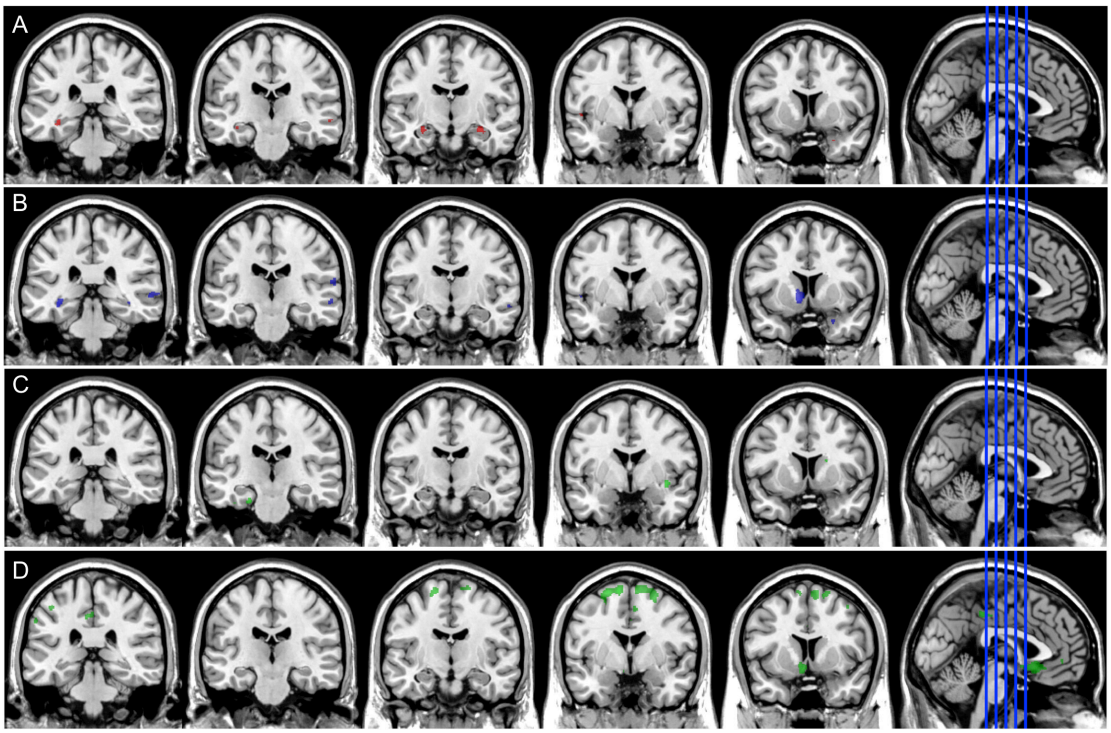

Figure 4 Individual subject's averaged (A) qT1 in right hippocampus and (B) qT2 in left paraphippocampus areas (based on the significant cluster in the longitudinal comparison) in AD, showing a trend of increase in qT1 / qT2 over time. For each line, the starting point (the left end) is determined by the subject's baseline MMSE score and the qMRI values at baseline. The end point of each line is set by the subject's follow-up MMSE score and the qMRI values at follow-up.